Ethylene Intersystem Crossing Caught in the Act by Photofragment Sulfur Atoms

Chaya Weeraratna, Chandika Amarasinghe, Baptiste Joalland[#]* and Arthur G. Suits*

Department of Chemistry, University of Missouri, Columbia, MO 65211 USA

ABSTRACT

Ethylene, C_2H_4, the simplest π-bonded molecule, is of enormous fundamental and commercial importance. Its lowest triplet state, in which the CH_2 moieties occupy perpendicular planes, is well known from theory but there has been no definitive experimental observation of this species. Here, velocity map imaging of the sulfur atoms in ethylene sulfide (c-C_2H_4S) photodissociation at 217 nm is used to reveal the internal state distribution of co-product ethylene. While both S (^{1}D) and S (^{3}P) translational energy distributions display three distinct regions that find their origins in singlet and triplet excited states of c-C_2H_4S, respectively, the S (^{3}P) distribution is dominated by a fourth, low-recoil region. In this region, the distribution is fully isotropic at a recoil of 9±1 kcal/mol, corresponding to the opening of the triplet ethylene channel. Multireference calculations suggest that this photodissociation pathway is mediated by a hot, transient biradical CH_2CH_2S that strongly favors CH_2 hindered rotations in the pre-dissociated complex. This photochemical ring-opening mechanism is invoked to account for the vibrational features observed in this low-recoil region, which are attributed to triplet ethylene relaxing to the torsional saddle point on the ground state singlet surface. This study thereby gives for the first time the experimental confirmation of an adiabatic singlet-triplet splitting of 66±1 kcal/mol and a torsional barrier height of 64±1 kcal/mol in ethylene.

1. Introduction

The dynamics of a photochemical reaction map the timeline of a molecule, energized by the absorption of one or several photons, to its asymptotic products. If one of the products is an atom, the direction and magnitude of its recoil velocity directly report on the internal energy of the co-fragment owing to energy and momentum conservation. In this case, the translational energy and angular distributions tell the story of the fragmentation dynamics, but they can also reveal the co-product electronic states, isomeric composition, and even its internal dynamics. This is entirely analogous to photoelectron spectroscopy which is used to reveal important information on the internal states of cations by capturing the velocities of the ejected electrons.[1, 2] Velocity map ion imaging,[3-5] coupled with high-level electronic structure methods, offer a powerful means of obtaining such information. With measurements on S (^{3}P) and S (^{1}D), this strategy is applied here to study the dynamics of ethylene sulfide, c-C_2H_4S, after photoexcitation to its lowest-energy absorption band in the UV (217 nm), yielding insight into the electronic states participating in the decay dynamics, and also elusive properties of the undetected ethylene co-product at high internal energies.

Previous photodissociation studies of ethylene sulfide have mostly been carried out at 193 nm (6.41 eV).[6-10] Using laser-induced fluorescence spectroscopy to probe S (^{1}D), Kim et al.[6] measured a recoil anisotropy parameter (β) close to unity, indicating that the transition is predominantly parallel to the C_2 axis and corresponds to a symmetric elongation of both C-S bonds. In a photofragment translational spectroscopy study using electron impact ionization, Felder et al.[7] studied the competing dissociating pathways and observed the highest contribution from hydrogen loss (~80%) yielding H + C_2H_3S. A 10% yield for the S + C_2H_4 channels was inferred. In a photofragment translational energy spectroscopy study with synchrotron radiation, Qi et al.[9] identified the S (^{3}P, ^{1}D) + C_2H_4 channels as the dominant pathways (see Scheme 1). By selectively tuning the ionization energy of the probe, distinct translational energy distributions for S (^{3}P) and S (^{1}D) were obtained. For the S (^{3}P) photofragment, a peak tentatively ascribed to triplet ethylene ($^3A_1$)[8] was identified, giving a lower bound estimate of 58 ± 3 kcal/mol for the adiabatic singlet-triplet splitting of ethylene. The branching ratio of the three channels S (^{1}D) + C_2H_4 (^1A_g), S (^{3}P) + C_2H_4 (^1A_g), and S (^{3}P) + C_2H_4 ($^3A_1$) was measured to be 41:57:2.

Scheme 1. S (^{3}P) and S (^{1}D) dissociation channels of ethylene sulfide and corresponding available energies (E_{avail}) of the 217 nm photofragments

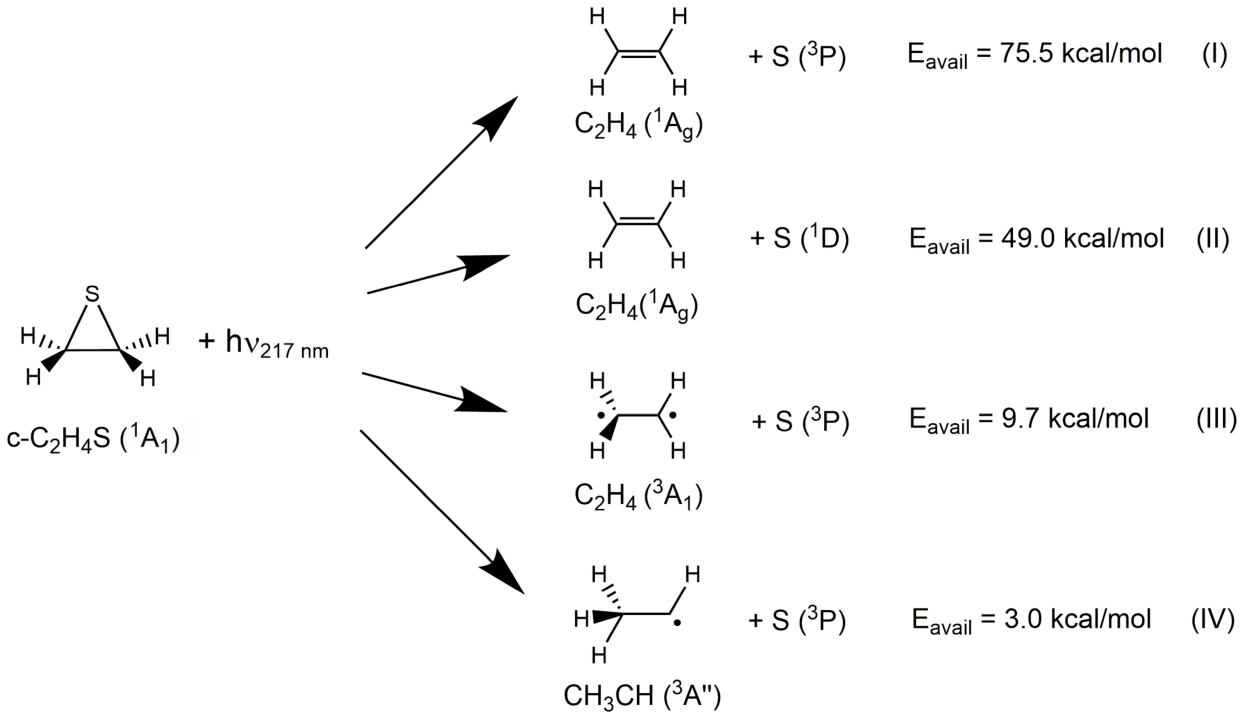

For the S (^{3}P) and S (^{1}D) channels accessible at 217 nm (Scheme 1), the co-product C_2H_4 is found either in the ground state (singlet) or first excited state (triplet) of ethylene or converted to ethylidene, CH_3CH. As surprising as this might seem and as discussed above, there is today no direct experimental measurement of the heats of formation of triplet ethylene, C_2H_4 (ã $^3A_1$), and ethylidene, CH_3CH ($^3A''$), whereas those of ground state ethylene, C_2H_4 ($\tilde{X}$ ^1A_g), and ethylene sulfide, C_2H_4S ($\tilde{X}$ $^1A_1$), as well as the energy levels of S (^{3}P) and S (^{1}D) are precisely known.[11, 12] For channels III and IV, the E_{avail} values reported above are therefore derived from the thermochemical values calculated by Nguyen et al,[13] which represent some of the most accurate theoretical predictions available in the literature today. These were deemed inconsistent with the values for triplet ethylene inferred by Qi et al.[8] As we will show below, the present study uncovers the vibronic levels at play in the intersystem crossing of ethylene and thus reconciles experiment with theory.

Ethylene C_2H_4 has been scrutinized many times in experimental and theoretical studies.[8, 13-19] It is the simplest π-bonding molecule and is used as a prototype for studying more complex unsaturated hydrocarbons.[20, 21] The ground state ($\tilde{X}\ ^1A_g$) properties of this planar polyatomic system, which belongs to the D_{2h} point group, are well understood,[22, 23] while there are only a limited number of studies regarding the excited states. Excitation of an electron from the bonding π orbital to the antibonding π* orbital deposits the system on a saddle point of the potential energy surface (PES) of its first triplet excited state, which must twist the two planes formed by the CH_2 groups at 90° to reach the minimum ($\tilde{a}\ ^3A_1$) pertaining to the D_{2d} point group.[19, 24] Peyerimhoff et al.[17] computed the triplet-singlet intersystem crossing rates for different vibrational states and concluded that radiationless transitions dominate the intermolecular energy transfer when compared to de-excitation from phosphorescence. From coupled-cluster CCSD(T) energies extrapolated to the complete basis set limit, Dixon and coworkers[13] derived the heat of formation ($\Delta H_f°$) of the triplet excited state of ethylene and the vertical and adiabatic singlet-triplet energy separation, along with $\Delta H_f°$ of ethylidene CH_3CH. The results are in close agreement with other highly accurate calculations based on Quantum Monte Carlo methods,[25, 26] but show a marked difference from the experimental ones of Qi et al.,[8] suggesting an overestimation of the stability of the triplet state in the experiment either owing to misassignment or imprecise calibration or fitting.

2. Experimental and Computational Methods

2.1 Experimental Section

A detailed description of the experimental setup, with laser geometries and modifications to the velocity map imaging configuration, were recently presented.[27-30] Two vacuum chambers, a source chamber and a main chamber, are each differentially pumped by magnetic-bearing turbomolecular pumps. A piezoelectric disk valve, operated at 10 Hz with a nominal pulsed width of 120 microseconds and 1050 torr backing pressure, is mounted in the source chamber. The position of the valve is adjusted to let the isentropic core of the pulsed supersonic expansion enter the main chamber via a 0.5 mm skimmer after travelling for 3 cm, providing a cold (~1 K) molecular beam. In the main chamber, the DC slice velocity map imaging setup[27] consists of an

ion optics arrangement with four ion lenses in one end of a time-of-flight tube, and a position sensitive microchannel plate (MCP) coupled to a phosphor detector in the other end. Between the repeller and extractor lenses (first and second lenses), the molecular beam is intersected at right angles by the pump and the probe laser beams. Along the time-of-flight axis, a sharp velocity focusing of the ion cloud expansion is achieved by applying optimum voltages to the ion lenses. The MCP was gated with a pulse duration of 70 ns to image the central slice of the sulfur ion cloud. The images were captured by a CCD camera and analyzed with the Finite Slice Analysis Program (FINA).[31, 32]

A molecular beam of ~5% ethylene sulfide was produced by passing helium through a glass bubbler containing liquid ethylene sulfide (Sigma Aldrich, 98%). The target molecule was dissociated at 217 nm and the S (^{1}D) and S (^{3}P) photoproducts were probed by the following schemes:

$$S\ (^1D)\ (3s^2\ 3p^4) + h\nu \rightarrow S\ (^3S_0)\ (3s^2 3p^3(4S_0)4s) + h\nu \rightarrow S^+\ (216.9\ nm)\ ^{30}$$

$$S\ (^3P_2)\ (3s^2\ 3p^4) + 2h\nu \rightarrow S\ (^3P_1)\ (3s^2 3p^3(^4S^0)5p) + h\nu \rightarrow S^+\ (308\ nm)\ ^{33}$$

217 nm photons were produced by pumping a dye laser with the second harmonic of a Nd:YAG laser (532 nm). The fundamental of the dye laser (DCM in DMSO) was frequency tripled to obtain the output at 217 nm. The laser was focused to the interaction region through a 230 mm focal length fused-silica lens and the power was kept at ~1 mJ/pulse. The probe laser beam at 308 nm was obtained by frequency doubling a second dye laser pumped by a Nd:YAG laser, (mixture of Rhodamine B and Rhodamine 101). The probe (~0.5 mJ/pulse) was fired with a ~20 ns delay to obtain the two-color signal and its linewidth (~0.05 cm^{-1}) was scanned through the Doppler profile to capture the entire image.

2.2 Computational Methods

In synergy with the experimental work, a number of multireference ab initio calculations were performed to provide insights in the electronic and vibrational states participating in the

photochemical relaxation processes as well as to examine the possible role of transient isomers in mediating the outcome of the photochemical reactions.

One-dimensional potential energy surfaces (potential energy cuts, PECs) were calculated along the C_2 axis of the parent molecule c-C_2H_4S ($\tilde{X}$ $^1A_1$) for all the singlet and triplet states converging to the S + C_2H_4 asymptotes accessible at 217 nm. These calculations were performed with the extended multi-state complete active space second-order perturbation theory (XMS-CASPT2), an efficient multireference approach for treating dynamical electron correlation.[34] Nine singlet and six triplet states were first mixed in a state-averaged complete active space self-consistent field (CASSCF)[35] wave function with an active space of six electrons in nine orbitals (6/9). The selected orbitals comprised the $8a_1$ (bonding, C_2H_4 (π) – S ($3p_z$)), $4b_2$ (bonding, C_2H_4 (π^*) – S ($3p_x$)), and $3b_1$ (nonbonding, S ($3p_y$)) occupied valence orbitals, the S (4s), S (4p), and S ($3d_{z2}$) Rydberg orbitals, and the $9b_2$ virtual orbital, which is key to describe the only valence excited state ($^1A_2$, dark state). A level shift of 0.4 a.u. was used and the geometry of the singlet ground state minimum optimized with the M06-2X[36] functional was not relaxed.

Additional PECs were calculated to examine (i) the ring-opening internal coordinate that links the parent c-C_2H_4S geometry to the biradical CH_2CH_2S structure ; (ii) the CH_2 rotation, i.e., the torsional mode of the ethylene moiety. These calculations were done at the CASSCF level by averaging the two lowest singlets and triplets without geometry constraints. A larger active space made of ten electrons in eleven orbitals (10/11) was necessary to account for the changes in the π and σ systems of the ethylene moiety along both coordinates. For the ring-opening coordinate, the S atom was moved parallel to the C-C bond while keeping all the other coordinates fixed with respect to the singlet ground state geometry optimized at the M06-2X level. For the torsion coordinate, a full geometry optimization on the lowest triplet surface was performed at the MP2[37] level and used as input geometry for the CASSCF evaluations.

Single-point XMS-CASPT2 calculations were also performed based on the geometries of minima and saddle points associated with the CH_3CHS and CH_2CHSH isomers, which were optimized on both singlet ground state and first triplet state PESs with the M06-2X functional. The number of averaged states was reduced to four singlets and three triplets and an active space

of six electrons in six orbitals (6/6) was used with no geometry constraints. The energies were not corrected for the zero-point energy contributions.

Multireference (XMS-CASPT2 and CASSCF) and MP2 calculations were done with MOLPRO[38] and M06-2X calculations with Gaussian09.[39] Dunning's aug-cc-pVTZ, basis set,[40, 41] denoted as AVTZ in the following, was used for all atoms throughout.

3. Results

3.1 DC slice velocity map imaging

The S (^{1}D) and S (^{3}P) images with the corresponding translational energy distributions P(E_T) and angular distributions, obtained as described in Methods, are shown in Figure 1. Angular distributions are characterized by the anisotropy parameter β, which relates to the angle between the transition dipole moment (μ) and the recoil direction. With limits of 2 for parallel transitions

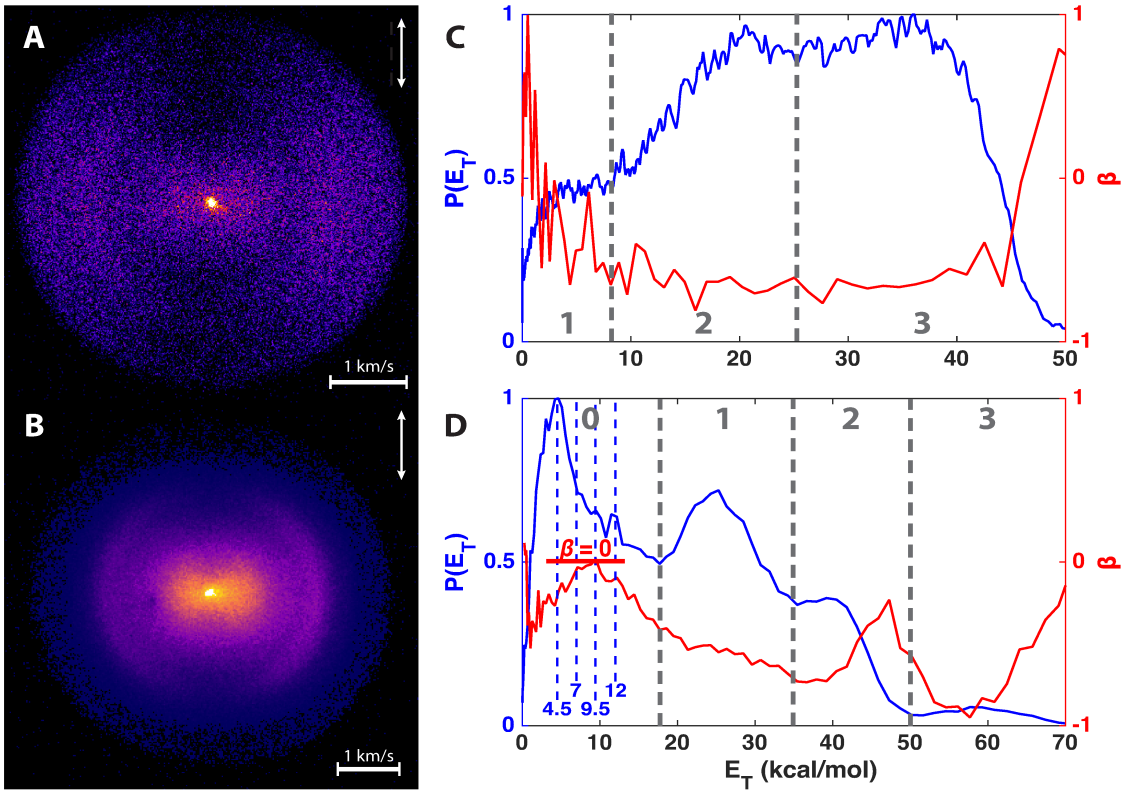

Figure 1. DC slice images of S (^{1}D) (A) and S (^{3}P) (B) for the photodissociation of ethylene sulfide c-C_2H_4S at 217 nm, along with translational energy distributions **P(E_T)** (blue) and anisotropy parameters ***β*** (red) (C, D). In region 0 of the S (^{3}P) **P(E_T)**, dashed lines separated by 2.5 kcal/mol plot out the vibronic levels in the intersystem crossing region of ethylene.

and -1 for perpendicular transitions, β is obtained by fitting the data to $I(\theta) \propto [1+\beta P_2(\cos\theta)]$,[42] with θ the angle between the laser polarization axis and the recoil direction and P_2 the second order Legendre polynomial.

The S (^{1}D) data exhibit three recoil regions: 0-8 kcal/mol (region 1), 8-25 kcal/mol (region 2), and 25-50 kcal/mol (region 3). In region 3 the maximum translational energy matches the available energy of the S (^{1}D) + C_2H_4 (^1A_g) pathway (I). β falls from 0 at zero recoil down to ~ -0.6 at E_T = 8 kcal/mol and remains then steady throughout regions 2 and 3. Table 1 summarizes the β values averaged over each region, as well as those from the earlier DC slice imaging study with 193 nm photoexcitation. The S (^{1}D) $P(E_T)$ at 217 nm shows remarkable similarities with previous work at 193 nm[9, 10] where three analogous components were also observed. However, the transition moment was mainly parallel to the recoil direction whereas in the present study it is mainly perpendicular.

Table 1. Anisotropy parameter β in the regions of S (^{1}D) / S (^{3}P) fragment recoil for 217 nm and 193 nm excitation wavelengths. 193 nm values from Townsend et al. [Ref. 12]

Photo-fragment	Wavelength	β			
		Region 0	Region 1	Region 2	Region 3
S (^{3}P)	217 nm	-0.31	-0.55	-0.64	-0.62
S (^{1}D)	217 nm	-	-0.38	-0.62	-0.61
	193 nm	-	0.6	1.0	1.4

The S (^{3}P) data also shows perpendicular angular distributions with beta values ranging from 0 to -0.9. Four recoil regions were identified: 0-18 kcal/mol (region 0), 18-35 kcal/mol (region 1), 35-50 kcal/mol (region 2), and 50-70 kcal/mol (region 3). For region 3, little flux was measured compared to regions 0, 1, and 2, and β varies from -0.9 at the center of this region to 0 on its wings. The velocity flux peaks at 5, 25, and 40 kcal/mol in region 0, 1, and 2, respectively, and the $P(E_T)$ shows an overall decrease in intensity from low to high recoil. In region 0, β changes

from -0.4 to 0 for recoil of 0 and 9 kcal/mol, and then steadily decays to -0.7 as recoil reaches its peak in region 2 located at 40 kcal/mol. The $P(E_T)$ data are largely consistent with the previous report on 193 nm synchrotron studies, although here the DC slice velocity map imaging technique allows us to highlight additional detail as discussed below.

3.2 Ab initio calculations

The PECs of the 15 states converging to the S (^{3}P), S (^{1}D), and S (^{1}S) asymptotes are shown in Figure 2 as a function of the distance between S and the center of the CC bond ($R_{S\text{-}X}$). At first glance, there are only three asymptotes but the highest one gathers three different ones: C_2H_4 ($^1A_1$) + S (^{1}S) (singly degenerate), C_2H_4 ($^1B_2$) + S (^{3}P) (triply degenerate), and C_2H_4 ($^3B_2$) + S (^{3}P) (triply degenerate). The geometry of C_2H_4 was not relaxed either to its ground state singlet or triplet geometries – a deliberate choice – so that these PECs can be viewed as how the S atom experiences the dissociation early in the dynamics. The dissociation towards C_2H_4 ($^3B_2$) + S (^{3}P), which occurs on a singlet surface, is permitted at 217 nm only if triplet ethylene relaxes to the twisted geometry of its global minimum, while the planar singlet excited state of ethylene (V state) is out of reach.

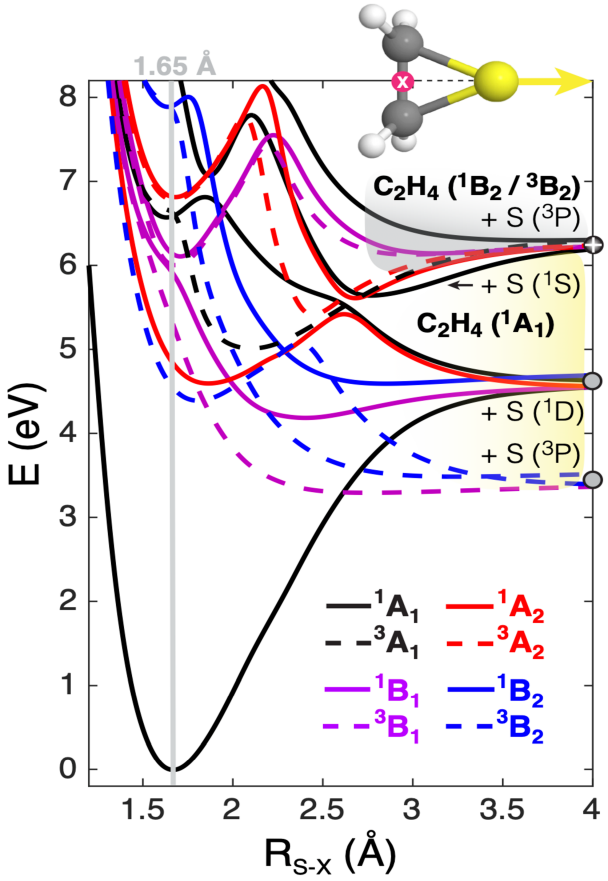

Figure 2. Potential energy cuts in the C_{2v} representation for the nine singlet and six triplet states of c-C_2H_4S converging to the S (^{3}P), S (^{1}D), and S (^{1}S) asymptotes accessible at 217 nm and 193 nm. $R_{S\text{-}X}$ denotes the distance between the S atom and the center of the C-C bond. All other coordinates are fixed to the singlet ground state optimized geometry. Energies are evaluated at the SA15-CASPT2(6/9)/AVTZ level.

These XMS-CASPT2 calculations were assessed both at the dissociation limit and in the Franck-Condon region. Table 2 reports the asymptotic values ($R_{S\text{-}X}$ = 20 Å) for an ethylene geometry relaxed to its planar singlet ground state minimum. SA15-CASPT2(6/9) overestimates the experimental bond dissociation energies by only ~0.2 eV. The calculated excitation energies of

the singlet-singlet transitions are compared with the experimental and MRCI values of Holland et al.[43] in Table 3. All the transitions involve Rydberg excited states with small to moderate oscillator strength, with the exception of the lowest A_2 valence state, which is spin forbidden. Again, SA15-CASPT2(6/9) compares well with the experimental values, i.e., within 0.2 eV, except for the two highest transitions towards the third and fourth A_1 states, which are overestimated by about 1 eV. These two states correspond to transitions to S (3d) and S (5p) Rydberg orbitals that were not included in the active space for pragmatic reasons, as this region of the absorption spectrum is particularly congested: Holland et al. reported seven states in the [7.53-7.83] eV window (at the MRCI level) involving not only S (3d) orbitals but also S (4s), S (5p), and S (4d) orbitals.[43] These states, which converge adiabatically to higher dissociation asymptotes and lie beyond the photoexcitation energies of 5.71 eV (217 nm) and 6.42 eV (193 nm), are not expected to participate in the dynamics. In Table 3 are also reported the three singlet-singlet transitions calculated at the SA7-CASPT2(6/6) level, which are highly consistent with the experimental ones and those obtained at the SA15-CASPT2(6/9) level.

Table 2. Bond dissociation energies of ethylene sulfide c-C_2H_4S in eV (kcal/mol).

Asymptote	EXP	SA15-CASPT2(6/9)
C_2H_4 (^1A_g) + S (^3P)	2.44 (*56.3*)	2.58 (*59.7*)
C_2H_4 (^1A_g) + S (^1D)	3.59 (*82.8*)	3.80 (*88.0*)
C_2H_4 (^1A_g) + S (^1S)	5.55 (*128.0*)	5.65 (*130.8*)

Table 3. Spectral assignment and energies in eV of the singlet-singlet transitions of c-C_2H_4S. Experimental and MRCI values from Holland et al. [Ref. 43] unless stated otherwise.

Transitions	EXP	MRCI	SA15-CASPT2(6/9)	SA7-CASPT2(6/6)
$3b_1 \longrightarrow 9b_2$ A_2	4.7[a] - 5.2[b]	5.44	4.89	4.86
$3b_1 \longrightarrow 4sa_1$ B_1	5.84	6.16	5.98	5.85
$3b_1 \longrightarrow 4pa_1$ B_1	5.91	6.33	6.17	6.05
$3b_1 \longrightarrow 4pb_1$ A_1	6.45	6.56	6.57	-
$3b_1 \longrightarrow 4pb_2$ A_2	6.79	6.86	6.83	-
$3b_1 \longrightarrow 3db_1$ A_1	7.48	7.60	8.66	-

$3b_1 \longrightarrow 3da_2$ B_2	7.59	7.53		7.87	-
$3b_1 \longrightarrow 5pb_1$ A_1		7.82	7.78	8.99	-

[a] Ref. 44 and [b] Ref. 45

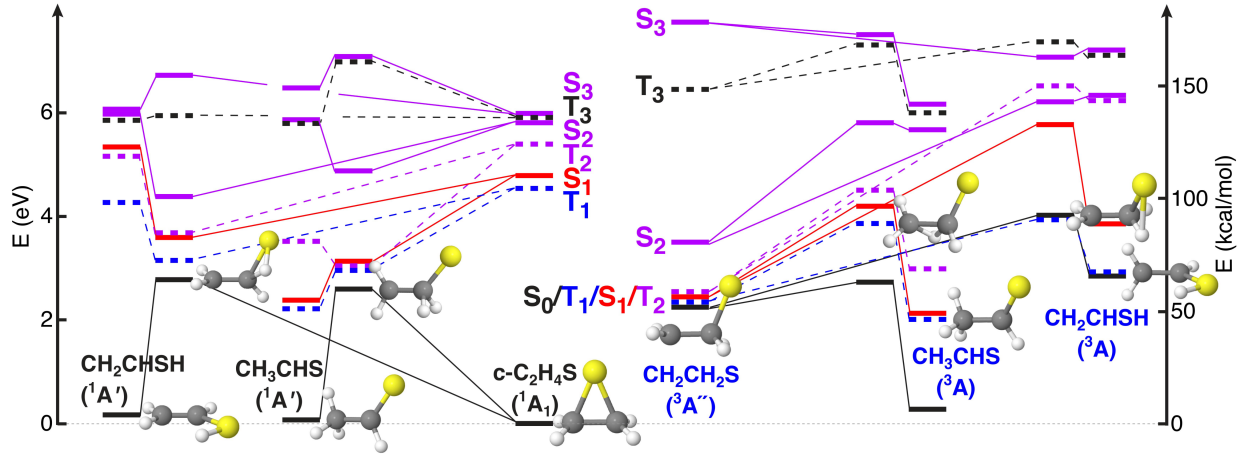

Figure 3: Energy diagram linking ethylene sulfide c-C_2H_4S (left) and biradical CH_2CH_2S (right) to the CH_3CHS and CH_2CHSH isomers. Geometries optimized on the singlet ground state (left) and the first triplet state (right) with the M06-2X functional. Energies determined at the SA7-CASPT2(6/6)/AVTZ level of theory with no zero-point energy correction.

During the photochemical relaxation processes, the possibility for interconversion to the CH_3CHS and CH_2CHSH isomers cannot be ruled out, although to-date no evidence has been shown that these species play a role in the S channels specifically. The key transient structure here is the biradical CH_2CH_2S, as can be seen in the energy diagram in Figure 3. After internal conversion from S_2 to S_1, the biradical CH_2CH_2S is expected to play a major role in branching out with an internal energy of 3-4 eV, i.e., about 3000 K per vibrational mode. With such a high internal energy, nearly

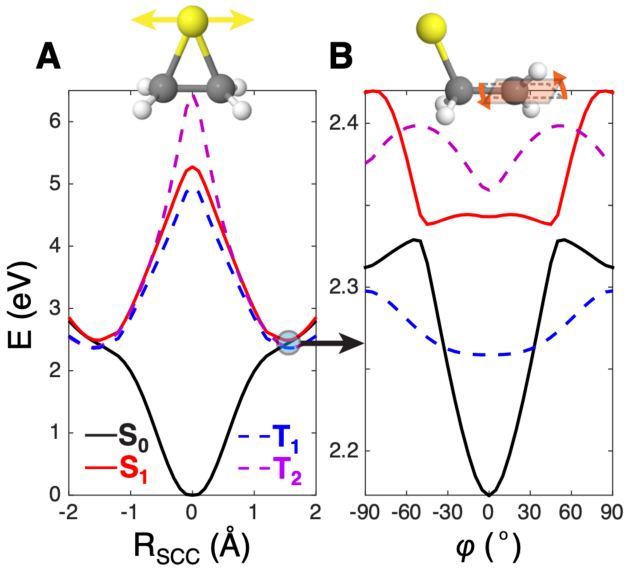

Figure 4: PECs of S_0, S_1, T_1, and T_2 along the ring-opening coordinate R_{SCC} (A) and the CH_2 torsional coordinate ψ (B). Energies determined at the SA4-CASSCF(10/11)/AVTZ level of theory. Note the change of energy scale between A and B.

anything could happen in terms of interconversion. Figure 3 shows nevertheless that interconversion to CH_3CHS is particularly favorable because the geometry of the biradical minimum is very close to the TS between c-C_2H_4S and CH_3CHS on the ground state singlet surface. By seeking for minimum energy conical intersections between S_0 and S_1 and between S_0 and T_1 in the biradical region, we found one of each with 45° and 90° torsional angle of for the ethylene moiety, respectively. Figure 4 illustrates these findings and further shows that the CH_2 group on the opposite side of S can be considered as a free rotor while coupling all the S_0, S_1, T_1, and T_2 states.

4. Discussion

Both experimental and theoretical results show evidence that the initial excitation with a 217 nm photon occurs on the $^1B_1$ state (S_2), whereas at 193 nm the first excited $^1A_1$ state is initially populated (S_4). The transition at 217 nm is perpendicular and corresponds to the promotion of a $3b_1$ electron to the S (4s) Rydberg orbital while the transition at 193 nm is parallel and corresponds to the promotion of the same electron to the S ($4pb_1$) orbital.

To identify the states at the origin of the three regions in the P(E_T) of S (^1D), we invoke the PECs in Figure 2 and the measured angular distributions in Table 1. Because $^1B_2$ is more repulsive than $^1B_1$, the fastest S (^1D) fragments (Region 3) are likely to arise from rapid internal conversion to the $^1B_2$ state followed by dissociation along that surface, while for region 2 the dissociation occurs directly on the $^1B_1$ surface. The steady β trend throughout these two regions supports this assignment, as well as their similar intensities. Region 1 must arise from the dark $^1A_2$ state. In this case, vibronic interactions due to asymmetric stretching will facilitate the relaxation to C_s symmetry where the $^1B_1$ and $^1A_2$ states both become A″ while the $^1B_2$ state becomes A′.

The S (^3P) data exhibit much richer detail. Region 3 is strongly anisotropic and corresponds to a minor process owing to its relatively low intensity. The $^3B_2$ state is most likely at the origin of this well-defined region. Similar to the dissociation from the singlet surfaces, we argue that the peaks at 45 and 25 kcal/mol in region 2 and 1 must come from $^3B_1$ and $^3A_2$, respectively. However, two different mechanisms are likely to be overlapped, especially in region 1: besides the dissociation from the $^3A_2$ state responsible for the peak at 25 kcal/mol, the data suggest that there is a "continuum" linking region 2 to region 0. This continuum comes from dissociation

events occurring in the hot biradical CH_2CH_2S. Interestingly, recent theoretical studies on oxirane C_2H_4O concluded that nearly 80% of the population leads to the biradical structure within 20-25 fs after photoexcitation to the S_2 state.[46, 47] It is very likely that such ultrafast ring-opening reaction is taking place in c-C_2H_4S as well given the similarities of these systems.

Region 0 can be divided in two sub-regions, the dividing line standing at 9.5 kcal/mol where the angular distribution becomes completely isotropic ($\beta = 0$). For $E_T > 9.5$ kcal/mol, the dissociation occurs on the ground state and/or the biradical and leads to a (very) hot singlet C_2H_4 fragment. For $E_T < 9.5$ kcal/mol, the only possible explanation is the release of triplet ethylene. Although the ethylidene CH_3CH channel is accessible for $E_T < 3$ kcal/mol, no clear marker of this channel was found. The $P(E_T)$ peaks at 4.5 kcal/mol, and there are small vibrational structures at 7 and 9.5 kcal/mol, along with one at 12 kcal/mol on the other side of the isotropic line. This spacing corresponds to ~800 cm^{-1}, a value in line with the torsional mode frequency calculated in triplet ethylene.[17] This may in fact be the same feature as that reported by Qi et al. but if so, the resolution of the photofragment translational spectroscopy experiment with overlapping features at 193 nm did not permit an accurate determination of the precise location of the peak.

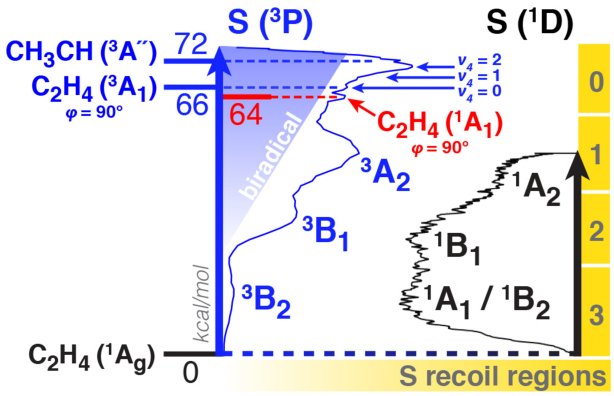

Figure 5. Translational energy distributions of S (^3P) and S (^1D) plotted against the internal energy of C_2H_4 and indicating the relevant excited states of c-C_2H_4S for each S recoil region.

We can now address the dynamical picture shown in Figure 5. With the migration of S towards one end of the C-C bond, i.e., the ring-opening reaction of the heterocycle, the $S_0/S_1/T_1/T_2$ states become degenerate and the CH_2 group on the opposite side of the C-C bond can freely rotate. Once the system has reached this point (again, in nearly 20-25 fs in C_2H_4O),[46, 47] either it will dissociate on the singlet surface to give triplet ethylene ($v_4 = 0, 1, 2$) + S (^3P) or it will dissociate on the triplet surface to give (hot) ground state ethylene + S (^3P). In both cases, this process is fast enough to conserve some of the incident anisotropy of the transition, although this anisotropy steadily decreases to the point where the triplet ethylene and singlet ethylene PESs

cross, i.e., where a cold triplet ethylene is released for E_T = 9.5 kcal/mol and β = 0. This description of the data is fully supported by accurate calculations of the adiabatic singlet-triplet transition in ethylene.[13, 25] The peak at 12 kcal/mol – a reminiscent feature in our data – is in consequence attributed to a portion of the metastable triplet ethylene that relaxes to the singlet by depositing the system on the CH_2-torsion saddle point of ground state ethylene. As stated by Gemein and Peyerimhoff, this saddle point corresponds to 24 quanta in the torsional mode ν_4 and the intersystem crossing from the T state of ethylene is rapid enough to be observed under our experimental conditions ($k = 7.7\times10^{10}$ s^{-1}) if no other vibrational mode is involved.[17]

Conclusions

Ethylene sulfide photodissociation at 217 nm reveals the dynamics of the formation of triplet ethylene. It appears as the low energy feature in the translational energy distribution of S (^{3}P) with an almost isotropic angular distribution. The cluster of vibrational features is attributed to the vibronic levels in the intersystem crossing between triplet and singlet ethylene. After a few tens of femtoseconds, the ring-opening reaction is completed and the system is locked up in the degenerate manifold of states in the biradical CH_2CH_2S region. The CH_2 group at the opposite of the S atom can store a significant amount of the internal energy in hindered rotations that couple the triplet surface with the ground state. The dissociation occurs from both surfaces and leads to triplet ethylene (ν_4 = 0, 1, 2) and hot singlet ethylene, while a portion of the metastable triplet ethylene relaxes to the singlet by depositing the system on the saddle point for rotational isomerization. Thus, imaging the S (^{3}P) channel offers a remarkable viewpoint on the internal dynamics of co-product ethylene C_2H_4.

AUTHOR INFORMATION

Corresponding Authors*

suitsa@missouri.edu

joallandb@wayne.edu

Present addresses

[#]Department of Chemistry, Wayne State University, Detroit, MI 48202 USA

ACKNOWLEDGMENT

This work was supported by the NSF under award number CHE-1665207 and by the ARO under award W911NF-1910283.

REFERENCES

1. Turner, D. W., Molecular photoelectron spectroscopy. *Philos. Trans. Royal Soc. A, Mathematical and Physical Sciences* **1970**, 7-31.

2. Shirley, D. A. *JOM Journal of the Minerals Metals and Materials Society*; 1976.

3. Chandler, D. W.; Houston, P. L., Two-dimensional imaging of state-selected photodissociation products detected by multiphoton ionization. *J. Chem. Phys.* **1987,** *87* (2), 1445-1447.

4. Parker, D. H.; Eppink, A. T. J. B., Photoelectron and photofragment velocity map imaging of state-selected molecular oxygen dissociation/ionization dynamics. *J. Chem. Phys.* **1997,** *107* (7), 2357-2362.

5. Suits, A. G., Invited Review Article: Photofragment imaging. *Rev. Sci. Instrum.* **2018,** *89* (11), 111101.

6. Kim, H. L.; Satyapal, S.; Brewer, P.; Bersohn, R., Photodissociation dynamics of ethylene sulfide at 193.3 nm. *J. Chem. Phys.* **1989,** *91* (2), 1047-1050.

7. Felder, P.; Wannenmacher, E.; Wiedmer, I.; Huber, J. R., Photodissociation of thiirane in a molecular beam at 193 nm. *J. Phys. Chem.* **1992,** *96* (11), 4470-4477.

8. Qi, F.; Sorkhabi, O.; Suits, A. G., Evidence of triplet ethylene produced from photodissociation of ethylene sulfide. *J. Chem. Phys.* **2000,** *112* (24), 10707-10710.

9. Qi, F.; Sorkhabi, O.; Suits, A. G.; Chien, S.-H.; Li, W.-K., Photodissociation of Ethylene Sulfide at 193 nm: A Photofragment Translational Spectroscopy Study with VUV Synchrotron Radiation and ab Initio Calculations. *J. Am. Chem. Soc.* **2001,** *123* (1), 148-161.

10. Townsend, D.; Lee, S. K.; Suits, A. G., Orbital polarization from DC slice imaging: S (1 D 2) alignment in the photodissociation of ethylene sulfide. *Chem. Phys.* **2004,** *301* (2), 197-208.

11. Domalski, E. S., Selected Values of Heats of Combustion and Heats of Formation of Organic Compounds Containing the Elements C, H, N, O, P, and S. *J. Phys. Chem. Ref. Data* **1972,** *1* (2), 221-277.

12. Martin, W. C.; Zalubas, R.; Musgrove, A., Energy Levels of Sulfur, S i through S xvi. *J. Phys. Chem. Ref. Data* **1990,** *19* (4), 821-880.

13. Nguyen, M. T.; Matus, M. H.; Lester, W. A.; Dixon, D. A., Heats of formation of triplet ethylene, ethylidene, and acetylene. *J. Phys. Chem. A* **2008,** *112* (10), 2082-2087.

14. Altenloh, D. D.; Russell, B., Electric dichroism spectroscopy in the vacuum ultraviolet dimethylsulfide and thiiran. *Chem. Phys. Lett.* **1981,** *77* (1), 217-221.

15. Balko, B.; Zhang, J.; Lee, Y. T., Photodissociation of ethylene at 193 nm. *J. Chem. Phys.* **1992,** *97* (2), 935-942.

16. Cromwell, E. F.; Stolow, A.; Vrakking, M. J.; Lee, Y. T., Dynamics of ethylene photodissociation from rovibrational and translational energy distributions of H2 products. *J. Chem. Phys.* **1992,** *97* (6), 4029-4040.

17. Gemein, B.; Peyerimhoff, S. D., Radiationless transitions between the first excited triplet state and the singlet ground state in ethylene: A theoretical study. *J. Phys. Chem.* **1996,** *100* (50), 19257-19267.

18. Tseng, C.-M.; Lee, Y. T.; Ni, C.-K.; Chang, J.-L., Photodissociation Dynamics of the Chromophores of the Amino Acid Tyrosine: p-Methylphenol, p-Ethylphenol, and p-(2-Aminoethyl) phenol. *J. Phys. Chem. A* **2007,** *111* (29), 6674-6678.

19. Wang, X.; Turner, W. E.; Agarwal, J.; Schaefer III, H. F., Twisted Triplet Ethylene: Anharmonic Frequencies and Spectroscopic Parameters for C2H4, C2D4, and 13C2H4. *J. Phys. Chem. A* **2014,** *118* (35), 7560-7567.

20. Zechmann, G.; Barbatti, M.; Lischka, H.; Pittner, J.; Bonačić-Koutecký, V., Multiple pathways in the photodynamics of a polar π-bond: A case study of silaethylene. *Chem. Phys. Lett.* **2006,** *418* (4), 377-382.

21. Aponte, J. C.; Dillon, J. T.; Tarozo, R.; Huang, Y., Separation of unsaturated organic compounds using silver–thiolate chromatographic material. *J. Chromatogr. A* **2012,** *1240*, 83-89.

22. Duncan, J.; Wright, I.; Van Lerberghe, D., Ground state rotational constants of H2CCD2 and C2D4 and geometry of ethylene. *J. Mol. Spectrosc.* **1972,** *42* (3), 463-477.

23. Duncan, J.; McKean, D.; Mallinson, P., Infrared crystal spectra of C2H4, C2D4, and as-C2H2D2 and the general harmonic force field of ethylene. *J. Mol. Spectrosc.* **1973,** *45* (2), 221-246.

24. Lown, E. M.; Sidhu, K. S.; Jackson, A. W.; Jodhan, A.; Green, M.; Strausz, O. P., Detection and properties of triplet state thiiranes. *J. Phys. Chem.* **1981,** *85* (9), 1089-1091.

25. El Akramine, O.; Kollias, A. C.; Lester Jr, W. A., Quantum Monte Carlo study of singlet–triplet transition in ethylene. *J. Chem. Phys.* **2003,** *119* (3), 1483-1488.

26. Barborini, M.; Sorella, S.; Guidoni, L., Structural optimization by Quantum Monte Carlo: investigating the low-lying excited states of ethylene. *J. Chem. Theory Comput.* **2012,** *8* (4), 1260-1269.

27. Townsend, D.; Minitti, M. P.; Suits, A. G., Direct current slice imaging. *Rev. Sci. Instrum.* **2003,** *74* (4), 2530-2539.

28. Broderick, B. M.; Lee, Y.; Doyle, M. B.; Vasyutinskii, O. S.; Suits, A. G., Velocity distribution of hydrogen atom spin polarization. *J. Phys. Chem. Lett.* **2013,** *4* (20), 3489-3493.

29. Broderick, B. M.; Lee, Y.; Doyle, M. B.; Chernyak, V. Y.; Vasyutinskii, O. S.; Suits, A. G., Spin-polarized hydrogen Rydberg time-of-flight: Experimental measurement of the velocity-dependent H atom spin-polarization. *Rev. Sci. Instrum.* **2014,** *85* (5), 053103.

30. Weeraratna, C.; Amarasinghe, C.; Fernando, R.; Tiwari, V.; Suits, A. G., Convenient (1+1) probe of S(1D2) and application to photodissociation of carbonyl sulfide at 216.9nm. *Chem. Phys. Lett.* **2016,** *657*, 162-166.

31. Thompson, J.; Amarasinghe, C.; Foley, C.; Rombes, N.; Gao, Z.; Vogels, S.; van de Meerakker, S.; Suits, A., Finite slice analysis (FINA) of sliced and velocity mapped images on a Cartesian grid. *J. Chem. Phys.* **2017,** *147* (7), 074201.

32. Thompson, J.; Amarasinghe, C.; Foley, C.; Suits, A., Finite slice analysis (FINA)—A general reconstruction method for velocity mapped and time-sliced ion imaging. *J. Chem. Phys.* **2017,** *147* (1), 013913.

33. Suzuki, T.; Katayanagi, H.; Nanbu, S.; Aoyagi, M., Nonadiabatic bending dissociation in 16 valence electron system OCS. *J. Chem. Phys.* **1998,** *109* (14), 5778-5794.

34. Shiozaki, T.; Győrffy, W.; Celani, P.; Werner, H.-J., Communication: Extended multi-state complete active space second-order perturbation theory: Energy and nuclear gradients. AIP: 2011.

35. Werner, H. J.; Knowles, P. J., A second order multiconfiguration SCF procedure with optimum convergence. *J. Chem. Phys.* **1985,** *82* (11), 5053-5063.

36. Zhao, Y.; Truhlar, D. G., The M06 suite of density functionals for main group thermochemistry, thermochemical kinetics, noncovalent interactions, excited states, and transition elements: two new functionals and systematic testing of four M06-class functionals and 12 other functionals. *Theor. Chem. Acc.* **2008,** *120* (1-3), 215-241.

37. Møller, C.; Plesset, M. S., Note on an approximation treatment for many-electron systems. *Phys. Rev.* **1934,** *46* (7), 618.

38. Werner, H. J.; Knowles, P. J.; Knizia, G.; Manby, F. R.; Schütz, M., Molpro: a general-purpose quantum chemistry program package. *Wiley Interdiscip. Rev. Comput. Mol. Sci.* **2012,** *2* (2), 242-253.

39. Frisch, M. J.; Trucks, G. W.; Schlegel, H. B.; Scuseria, G. E.; Robb, M. A.; Cheeseman, J. R.; Scalmani, G.; Barone, V.; Petersson, G. A.; Nakatsuji, H. et al., *Gaussian 16 Rev. B.01*, Wallingford, CT, 2016.

40. Kendall, R. A.; Dunning Jr, T. H.; Harrison, R. J., Electron affinities of the first-row atoms revisited. Systematic basis sets and wave functions. *J. Chem. Phys.* **1992,** *96* (9), 6796-6806.

41. Dunning Jr, T. H.; Peterson, K. A.; Wilson, A. K., Gaussian basis sets for use in correlated molecular calculations. X. The atoms aluminum through argon revisited. *J. Chem. Phys.* **2001,** *114* (21), 9244-9253.

42. Zare, R. N., Photoejection dynamics. *Mol. Photochem* **1972,** *4* (1), 1.

43. Holland, D. M. P.; Shaw, D. A.; Walker, I. C.; McEwen, I. J.; Guest, M. F., The valence shell electronic states of ethylene sulphide studied by photoabsorption and ab initio multireference configuration interaction calculations. *Chem. Phys.* **2008,** *344* (3), 227-236.

44. DAVIS, R. E., Cyclic Sulfides. I. Ultraviolet Spectra of Ethylene Sulfides. *The Journal of Organic Chemistry* **1958,** *23* (2), 216-218.

45. Clark, L. B.; Simpson, W. T., Vacuum-Ultraviolet Studies of Sulfides. I. Spectral Correlations and Assignment of the NV Transitions. *J. Chem. Phys.* **1965,** *43* (10), 3666-3672.

46. Min, S. K.; Agostini, F.; Tavernelli, I.; Gross, E. K., Ab initio nonadiabatic dynamics with coupled trajectories: A rigorous approach to quantum (de) coherence. *J. Phys. Chem. Lett.* **2017,** *8* (13), 3048-3055.

47. Curchod, B. F.; Agostini, F.; Tavernelli, I., CT-MQC–a coupled-trajectory mixed quantum/classical method including nonadiabatic quantum coherence effects. *Eur. Phys. J. B* **2018,** *91* (7), 168.

TOC Graphic